metals

MDPI

Article

Effects of Cr_2N Precipitation on the Antibacterial Properties of AISI 430 Stainless Steel

Je-Kang Du [1,2,3], Chih-Yeh Chao [4], Yu-Ting Jhong [5], Chung-Hao Wu [4] and Ju-Hui Wu [2,5,6,*]

1 School of Dentistry, College of Dental Medicine, Kaohsiung Medical University, Kaohsiung 80708, Taiwan; dujekang@gmail.com
2 Department of Dentistry, Kaohsiung Medical University Hospital, Kaohsiung 80708, Taiwan
3 Ph.D. program, School of Dentistry, College of Dental Medicine, Kaohsiung Medical University, Kaohsiung 80708, Taiwan
4 Department of Mechanical Engineering, National PinTung University of Science and Technology, PingTung 91201, Taiwan; cychao@mail.npust.edu.tw (C.-Y.C.); richman720423@gmail.com (C.-H.W.)
5 Graduate Institute of Oral Hygiene, College of Dental Medicine, Kaohsiung Medical University, Kaohsiung 80708, Taiwan; steelwillpower0130@gmail.com
6 Department of Oral Hygiene, College of Dental Medicine, Kaohsiung Medical University, No. 100, Shih-Chuan 1st Road, Kaohsiung 80708, Taiwan
* Correspondence: wujuhui1020@gmail.com; Tel.: +886-7-3121-101 (ext. 7007); Fax: +886-7-3157024

Academic Editors: Harrie Weinans and Amir A. Zadpoor
Received: 12 February 2016; Accepted: 17 March 2016; Published: 24 March 2016

Abstract: Based on their mechanical properties and good corrosion resistance, some commercial Ni-Cr stainless steels have been widely applied as biomaterials, including the austenitic 304 stainless steel, the austenitic 316 stainless steel, the duplex 2205 stainless steel, and the ferritic 430 stainless steel. In order to reduce the occurrence of infections resulting from biomaterial implants, instruments, and medical devices, Cu^{2+} and Ag^{2+} ions have been added onto biomaterials for increasing the antibacterial properties, but they are known to damage biofilm. The occurrence of nanoparticles can also improve the antibacterial properties of biomaterials through various methods. In this study, we used *Escherichia coli* and analyzed the microstructures of American Iron and Steel Institute (AISI) 430 stainless steel with a 0.18 mass % N alloy element. During a lower temperature aging, the microstructure of the as-quenched specimen is essentially a ferrite and martensite duplex matrix with some Cr_2N precipitates formed. Additionally, the antibacterial properties of the alloy for *E. coli* ranged from 3% to 60%, consistent with the presence of Cr_2N precipitates. When aged at a lower temperature, which resulted in nano-Cr_2N precipitation, the specimen possessed the highest antibacterial activity.

Keywords: Cr_2N precipitation; antibacterial behavior; ferritic type stainless steel; *Escherichia coli*

1. Introduction

Due to their good mechanical properties, malleability, and wear resistance, metals are widely applied as bio-implant materials, such as fracture fixation devices or artificial joints in plastic surgery [1]. In particular, stainless steels and titanium alloys are commonly used in this application for their good corrosion resistance [2,3]. For example, the austenitic 304 and 316 stainless steels are used for coronary stents, bone replacement, fracture fixation, stents, hip stems, spinal implants, and cables. The duplex 2205 stainless steel is used in mini-screw implants in orthodontic dentistry. In addition, the ferritic 430 stainless steel is used in surgical and dental instruments. Meanwhile, titanium alloys are used in bone replacement, load-bearing sites, hip or dental prostheses, spinal cages, and artificial hip joints [4–10].

On the other hand, blood compatibility and bio-surface activity are major concerns in biomaterial application. Moreover, bacteria may adhere to the surface of medical devices, forming a biofilm that can cause postoperative infections. For biomaterial research, most studies have reported that ion

exchange could improve the antibacterial properties of the biomaterial for solid solutions to incorporate antibiotics into metals. Dong *et al.* [11] described an antibacterial method for production of inorganic antibacterial materials in which an antibacterial agent was produced based on the intrinsic antibacterial capacity of the metal using ion exchange, physisorption, or combination with SiO_2 or other porous materials through photocatalysis by TiO_2. Yan *et al.* [12] explained that binding of electropositive metal ions with amino groups and other electronegative ions in proteins and nucleic acids would result in more rapid degradation of proteins, blocking the metabolic functions of bacteria and thus achieving antibacterial effects. It is noted that the various antibacterial mechanisms could improve the antibacterial properties of a biomaterial. Li *et al.* [13] claimed that some precipitation of copper ions on the austenitic 304 stainless steel with 3.88 mass % copper resulted in antibacterial effects through inhibition of biofilm growth. Yang and Nan [14,15] also proposed that copper ions had excellent reducing capacity and could destroy the cell wall and membrane of *Escherichia coli* cells by binding with electrons in the bacteria, resulting in loss of the cytoplasm, oxidation of the nucleus, and death of the bacterial cells. Meanwhile, for the austenitic 304L stainless steel with added 4 mass % copper, Zhu *et al.* [16] found that the copper ions precipitated on the material surface, resulting in complete destruction of *E. coli* and *Staphylococcus aureus* cells. In addition, silver ions have also been added to the stainless steel for their antibacterial property. Chang [17] found that the addition of silver on 2205 duplex stainless steel would induce the release of silver ions and penetrate the cell walls of *E. coli* and *S. aureus*, resulting in suppression of metabolic function and cell death. Lin [18] also found that the addition of 0.03 mass % silver on the ferritic 430 stainless steel may increase the antibacterial rate to 80%. Various concentrations of silver added onto austenitic 316L stainless steel have been studied by Zeng [19]. Based on these studies, it seems that a higher silver proportion in the alloy would lend higher antibacterial capacity, ranging from 94% to 99%.

However, adding trace amounts of antibacterial alloy facilitates biocompatibility. Zhang *et al.* [20] added copper as an antibacterial factor into 304 stainless steel and showed that the protease of the experimental animal required a low concentration (3.9%) of copper ions to facilitate bone growth. Chu [21] found that good biocompatibility could also be achieved by adding a nitrogen alloy element. For example, good surface properties were obtained by adding nitrogen into diamond-like carbon, and good blood compatibility was achieved in platelet tests.

However, little information could be found about how adding nitrogen to the commercial stainless steel affected the antibacterial property. Therefore, the main purpose of the present study is to investigate the *E. coli* antibacterial properties of the ferritic 430 stainless steel with 0.18 mass % nitrogen. Moreover, in order to clarify the effects of the precipitation of the alloy on the antibacterial properties, a microstructural analysis of the present alloy is also performed.

2. Materials and Methods

2.1. Sample Preparation

The chemical composition of a commercial material (China Steel Corporation, Kaohsiung, Taiwan), designed as Sample A, is shown in Table 1. In the meantime, the alloys with various heat treatments, designated as Samples B to E, were prepared using commercial 430 stainless steel and nitrogen-chromium iron (Fe-30 mass % Cr-6.67 mass % N) in an air induction furnace. Being heated at 1000 °C/2 h, the ingots were hot-forged into rods with a diameter φ = 12 mm and length L = 180 mm. The rods were also heated at 880 °C for 1 h for solution heat treatment. Next, various aging processes were performed including 450 °C for 16 h, 500 °C for 4 h, and 550 °C for 1 h. After heated treatment, the rods were milled to diameter φ = 10 ± 0.05 mm, and cut into discs with a thickness t = 1.50 ± 0.05 mm.

Table 1. Chemical compositions (mass %) of 430 stainless steels used in the present study and the conditions of heat treatment.

Code \ Elements	Fe	Cr	Ni	N	C	Si	Mn	P	S	Solution Treatment/Aging
A	Bal.	17.22	0.48	-	0.10	0.65	0.72	0.03	0.02	880 °C/1 h + 450 °C/16 h
B	Bal.	17.01	0.51	0.18	0.08	0.70	0.68	0.03	0.01	880 °C/1 h
C										880 °C/1 h + 450 °C/16 h
D										880 °C/1 h + 500 °C/4 h
E										880 °C/1 h + 550 °C/1 h

2.2. Antibacterial Test

E. coli cultures were analyzed as follows. First, 400 µL *E. coli* solution was added and cultured (37 °C, 150 rpm, 3 h) in test tubes containing 20 mL of culture medium (Lysogeny Broth [LB]). The cells were then centrifuged (4 °C, 3000 rpm, 10 min), and the supernatant was discarded. Next, cells were resuspended in 1 mL LB broth, and the OD_{600} of the diluted bacterial solution was measured. One hundred microliters of the diluted 1×10^5 CFU/mL bacterial solution was dripped onto pre-sterilized steel, and the four-well chamber containing steel samples was placed in a thermostat at 37 °C for 20 h. Finally, the steel was rinsed, and the bacteria-smeared plates were collected. Steel test pieces were removed from the thermostat and washed with 1 mL PBS. The bacterial solution was diluted, and the OD_{600} was measured. The bacterial solution was serially diluted (10^3, 10^4, 10^5, 10^6, and 10^7), and the diluted solutions were used for repeated plate smearing and analysis of bacteriostatic effects.

2.3. Microstructure Analysis

Scanning electron microscope (SEM) were performed on JSM-6380 (JEOL, Tokyo, Japan) at 20 kV after etching in 5 mL HCl + 15 mL HNO_3 + 80 mL ethanol reagent. Electron microscopy specimens were prepared by means of a double-jet electropolisher with an electrolyte of 90% ethanol + 10% perchloric acid reagent. The polishing temperature was kept in the range from −20 to 0 °C, and the voltage was kept at 20 V. Transmission electron microscope (TEM) was performed on CM200 FEG (PHILPLIES, Hillsboro, OR, USA) and JEM-2000FX (JEOL, Tokyo, Japan) at 200 kV. The crystallographic analyses of precipitates and matrix were accompanied by a selected area diffraction pattern (SADP, JEOL, Tokyo, Japan) and bright field (BF) electron micrograph (JEOL, Tokyo, Japan).

3. Results

Based on the *E. coli* examinations, the amount of *E. coli* bacteria is between 1.88×10^6–5.2×10^6, as shown in Figure 1a. The *E. coli* bacterial rate is between 3% and 60%, as shown in Figure 1b. It is revealing that the addition of nitrogen on the ferritic 430 stainless steel would destroy *E. coli* cells, resulting in an increased bacterial rate. In Figure 1, it is also shown that the optimal bacterial rate would occur in Sample C, which has the lowest temperature aging process.

The microstructure of the specimen designated Sample A is a ferrite matrix and martensite duplex phase. A typical SEM electron micrograph, taken from the as-quenched specimen, is shown in Figure 2.

Figure 3a,b gives two BFs TEM electron micrographs, taken from the as-quenched specimen, indicating the ferrite and martensite phases, respectively. Figure 3c,d shows two SADPs, the foil normal widths are g = 011 ferritic matrix and g = 111 martensitic matrix, respectively. Based on the TEM examination, it is shown that some dislocations are formed within the ferrite matrix, as shown in Figure 3a. However, in Figure 3b, the density of dislocation within the martensite matrix would be higher than in the ferrite matrix. When 0.18 mass % nitrogen was added on the 430 stainless steel, the microstructure of the alloy was essentially similar to the commercial 430 stainless steel.

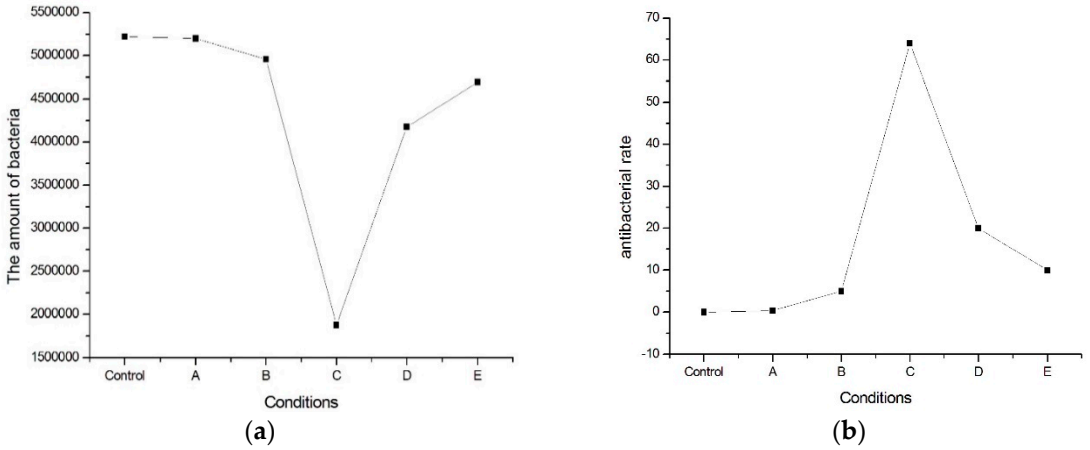

Figure 1. (**a**) The amount of *E. coli* bacteria and (**b**) *E. coli* bacterial rate of the present alloy with various heated treatments.

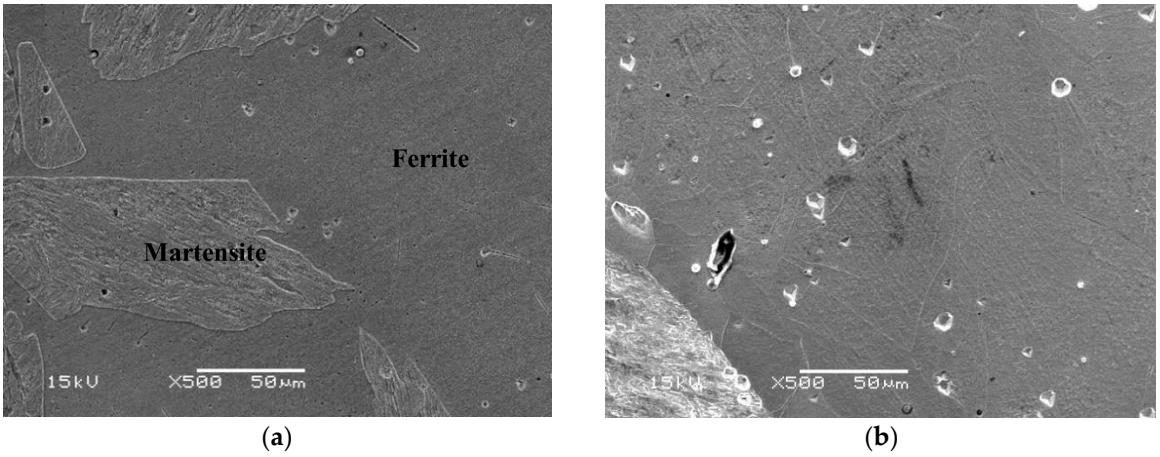

Figure 2. (**a**) SEM image of the as-quenched specimen; (**b**) revealing that the microstructure of the alloy was a ferrite matrix with 30% martensite phase.

A typical TEM electron micrograph is shown in Figure 4, which is a BF TEM electron micrograph of the as-quenched specimen designated Sample B. However, some extra fine precipitates are observed within the as-quenched specimen during the aging process, as shown in Figure 5a. Figure 5b shows a SADP taken from an area of the as-quenched specimen designated Sample C, aged at 450 °C for 16 h and covered with the precipitates and matrix. The foil normal width is g = 1120. It is revealing that the precipitates are Cr_2N nitride, which has an HCP structure with lattice parameters a = 0.278nm and c = 0.446 nm. Moreover, the particle size of the Cr_2N precipitate is between 3.57 nm and 7.14 nm. Increasing the aging temperature to 500 °C for 4 h, the microstructure of the specimens is essentially similar to Sample C. However, the particle size of the Cr_2N precipitate would increase in the range of 28.5–68.7 nm, as shown in Figure 6. When aged at 550 °C for 1 h, the morphology of the Cr_2N precipitate would become a rod type, as shown in Figure 7. It is noted that the presence of Cr_2N precipitates would be consistent with the antibacterial properties of the alloy for *E. coli*, and the smaller size of Cr_2N precipitation would result in a higher bacterial rate.

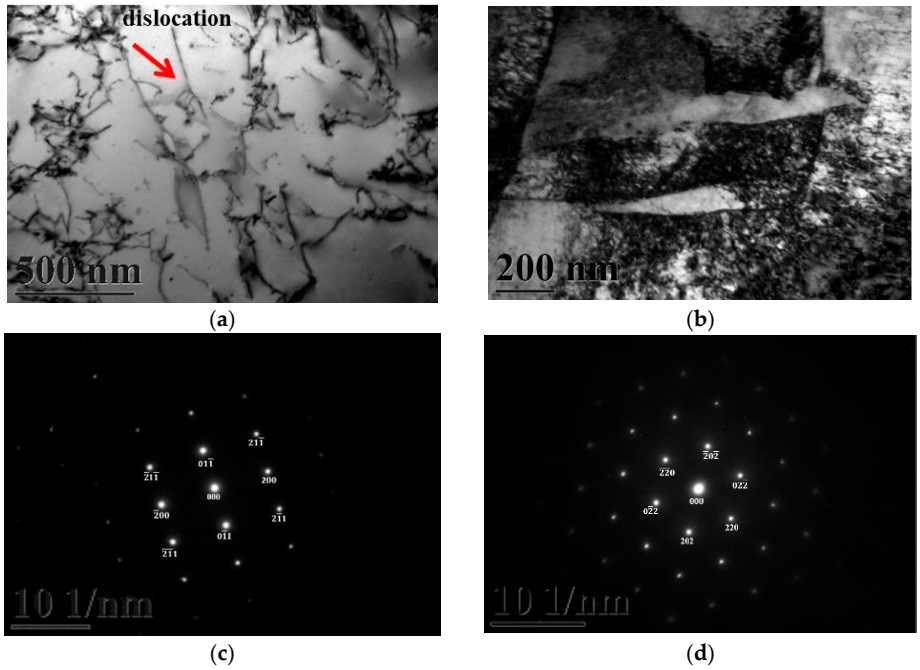

(**a**) (**b**) (**c**) (**d**)

Figure 3. TEM images of the as-quenched specimen (group A). (**a**) a BF image of the ferrite matrix; (**b**) a BF image of the martensite matrix; (**c**) a SADP of the ferrite matrix, and the foil normal is g = 011; and (**d**) a SADP of the martensite matrix, and the foil normal is g = 111.

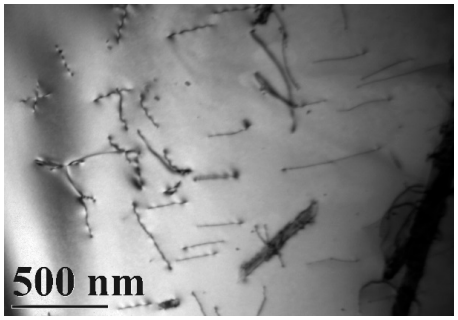

Figure 4. Bright-field TEM image of the as-quenched specimen (Sample B).

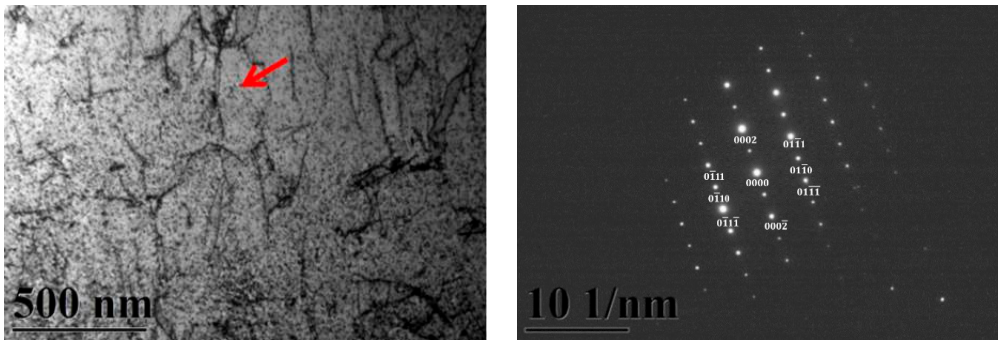

(**a**) (**b**)

Figure 5. TEM image of the specimen aged at 450 °C for 16 h (Sample C). (**a**) Bright-field image of the ferrite matrix; (**b**) SADP, revealing that g = 1120 was a Cr_2N precipitate. The arrow indicates the precipitated particles.

Figure 6. Bright-field TEM image of the specimen aged at 500 °C for 4 h (Sample D).

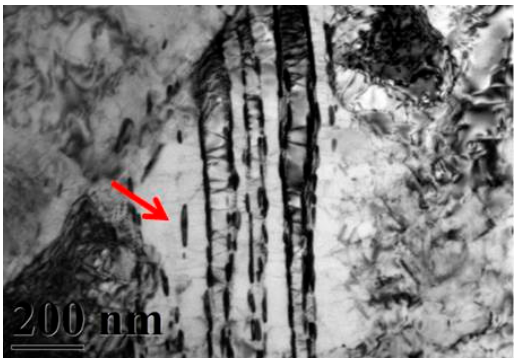

Figure 7. Bright-field TEM image of the specimen aged at 550 °C for 1 h (Sample E).

4. Discussion

The precipitates produced in this study were metal nanoparticles, which exhibited a grain size of 3.57–68.5 nm, as calculated from Figure 5. There are three main antibacterial mechanisms of metal nanoparticles. Díaz-Visurraga *et al.* [22] found that nanoparticles entered into bacteria cells to block bacterial anabolism and DNA replication, produced reactive oxygen species to oxidize bacterial cells and cause damage to membranes, and dissolved the bacterial cell membrane to change conductivity and alter the consuming power of protons in cells. However, the antibacterial element nitrogen is rarely added to metals; in most cases, nitrogen has been bound to organic compounds for antibacterial experiments. The antibacterial properties of nitrogen were also confirmed by the experimental results of Dunnill *et al.* [23], in which nitrogen was added into TiO_2 film by photocatalysis, and the results showed that this material killed 99.9% of *E. coli*. Zhang *et al.* [24] added nitrogen to medical polymers by plasma immersion ion implantation, thereby increasing both the amount of nitrogen bound to cellular proteins and the number of dead cells. These results suggested that antibacterial activity was increased after adding nitrogen. The precipitates from this alloy were nanoparticles that could induce cytotoxicity or enter into the cytoplasm through the cell membrane via an electrostatic interaction formed between the alloy and cell membrane [25–27]. These interactions would cause damage to the cell membrane and wall, resulting in gradual loss of cytoplasm, reduced metabolic and growth abilities, and eventual cell death [27].

In this study, after high-temperature solid solution treatment at 880 °C, the matrix of the alloy cast microstructure was in the α phase. According to chromium-iron binary phase diagrams [28], a Cr content of 17 wt. % results in the ferrite α phase. Aging treatment performed at 800 °C produced the α phase and precipitates, and the martensite phase was also observed. With increased aging time, the binding force between N and Cr increased, producing Cr_2N, which subsequently precipitated [29]. Shen *et al.* [30] performed aging treatments at 1050 °C for 1 h and 600–780 °C for 2 h for ferrite and martensite duplex stainless steel containing 11% Cr and observed stripe-like Cr_2N precipitates after

aging for 2 h at 650 °C. Sung *et al.* [29] performed aging at 1100 °C for 15 min using 430 ferrite stainless steel plates and found 130-μm martensite structures in the microstructure of ferrite. Mola *et al.* [31] performed hot rolling of 430 ferrite alloy with argon in a vacuum and found that martensite was formed in the microstructure of ferrite. Erneman *et al.* [32] added nitrogen to 347 austenitic stainless steel and examined changes in the precipitates after heat treatment. The results showed that after prolonged aging treatment, Cr_2N precipitates were produced due to increased binding between N and Cr. Additionally, the grain boundary thickened over time, and more Cr_2N precipitated from the grain boundary. The microstructure results for the precipitates and phases were similar to our current study.

In this study, the antibacterial element nitrogen was added into alloys and precipitated by aging treatment. The bacterial solution was then added, and the observed decrease in bacterial cell counts indicated the antibacterial properties of this precipitate [33,34]. In the experiment conducted by Chieh [35], if the content of the antibacterial element was not sufficient for precipitation on the surface, no antibacterial properties were observed. By adding a solid solution containing the antibacterial element, the amount of precipitate also increased over time during aging. However, as shown in Figure 1, Samples A and B had very low antibacterial activities, likely because the microstructures produced in Samples A and B had dislocations but no precipitates; thus, the presence of a precipitate was correlated with antibacterial activity. Compared with Samples A and B, Samples C–E exhibited dramatically different antibacterial activities, with Sample C showing the best antibacterial activities and a granular microstructure. In contrast, Samples D and E exhibited block-like and stripe-like structures, with the latter resembling a meteor shower, similar to the experimental results of Shi *et al.* [36]. In this prior study, heat treatment of the Fe-18Cr-12Mn-0.48N alloy was carried out, after which Cr_2N was produced by Cr binding with precipitated N. The original precipitates were granular and changed to a lamellar structure as the temperature increased. Van Landeghem *et al.* [37] calculated the diffusion of nitrides in ferrites and the growth of grains and grain boundaries. They found increased precipitation of nitride particles as the nitrogen concentration progressively increased in the solid solution. The density of Cr_2N particles was constant, and the equilibrium volume fraction of particles and the time at which coarsening began depended on the chromium content in the solid solution. Therefore, the size of precipitated grains grew with time. The gradually increasing size of precipitated grains may cause uneven antibacterial properties, and we conclude that the shape of the precipitates may be associated with antibacterial properties.

5. Conclusions

When 0.18 mass % nitrogen added on the 430 stainless steel, some Cr_2N precipitates were formed within the matrix with different morphologies during various heated treatments. Aged at 450 °C/16 h, Cr_2N precipitates would be nanoparticles with the size of 3.57–7.14 nm. In addition, the antibacterial rate of this specimen would be 60%. Upon increasing the aging temperature, the Cr_2N precipitates would increase. Moreover, the antibacterial rate of the specimen would decrease. It is implied that the Cr_2N precipitates were correlated with antibacterial effects toward *E. coli*, and the antibacterial rate ranged from 3% to 60%. However, it is noted that the present results have never been reported before.

Acknowledgments: This work was partially funded by a grant from the Ministry of Science and Technology, ROC (104-2314-B-037-057-MY2).

Author Contributions: Je-Kang Du and Yu-Ting Jhong conceived and designed the experiments; Je-Kang Du performed the experiments; Chih-Yeh Chao analyzed the data; Chung-Hao Wu contributed reagents/materials/analysis tools; Je-Kang Du and Ju-Hui Wu wrote the paper.

Conflicts of Interest: The authors declare no conflict of interest.

References

1. Gehrig, L.M. Orthopedic surgery. *Am. J. Surg.* **2011**, *202*, 364–368. [CrossRef] [PubMed]
2. Chen, Q.; Thouas, G.A. Metallic implant biomaterials. *Mater. Sci. Eng. R Rep.* **2015**, *87*, 1–57. [CrossRef]

3. Prasad, S.; Ehrensberger, M.; Gibson, M.P.; Kim, H.; Monaco, E.A. Biomaterial properties of titanium in dentistry. *J. Oral. Biosci.* **2015**, *57*, 1–8. [CrossRef]
4. Mahapatro, A. Bio-functional nano-coatings on metallic biomaterials. *Mater. Sci. Eng. C Mater. Biol. Appl.* **2015**, *55*, 227–251. [CrossRef] [PubMed]
5. Ren, L.; Yang, K. Bio-functional design for metal implants, a new concept for development of metallic biomaterials. *J. Mater. Sci. Technol.* **2013**, *29*, 1005–1010. [CrossRef]
6. Barrère, F.; Mahmood, T.A.; de Groot, K.; van Blitterswijk, C.A. Advanced biomaterials for skeletal tissue regeneration: Instructive and smart functions. *Mater. Sci. Eng. R Rep.* **2008**, *59*, 38–71. [CrossRef]
7. Geetha, M.; Singh, A.K.; Asokamani, R.; Gogia, A.K. Ti based biomaterials, the ultimate choice for orthopaedic implants—A review. *Prog. Mater. Sci.* **2009**, *54*, 397–425. [CrossRef]
8. Liu, X.; Chu, P.; Ding, C. Surface modification of titanium, titanium alloys, and related materials for biomedical applications. *Mater. Sci. Eng. R Rep.* **2004**, *47*, 49–121. [CrossRef]
9. Lyndon, J.A.; Boyd, B.J.; Birbilis, N. Metallic implant drug/device combinations for controlled drug release in orthopaedic applications. *J. Control. Release* **2014**, *179*, 63–75. [CrossRef] [PubMed]
10. Newson, T. *Stainless Steel for Hygienic Applications*; European Confederation of Iron and Steel Industries: Brussels, Belgium, 2003.
11. Dong, J.; Chen, S.; Lu, M.; Yang, K. History and current status of antibacterial material. *Mater. Rev.* **2004**, *18*, 41–46.
12. Yan, Y.; Zhao, Y. Inorganic antimicrobial materials. *Chem. Ind. Eng. Prog.* **2001**, *7*, 5–9.
13. Li, M.; Nan, L.; Xu, D.; Ren, G.; Yang, K. Antibacterial performance of a Cu-bearing stainless steel against microorganisms in tap water. *J. Mater. Sci. Technol.* **2015**, *31*, 243–251. [CrossRef]
14. Yang, K.; Lu, M. Antibacterial properties of an austenitic antibacterial stainless steel and its security for human body. *J. Mater. Sci. Technol.* **2007**, *23*, 333–336.
15. Nan, L.; Yang, W.C.; Liu, Y.Q.; Xu, H.; Li, Y.; Lu, M.; Yang, K. Antibacterial mechanism of copper-bearing antibacterial stainless steel against *E. coli*. *J. Mater. Sci. Technol.* **2008**, *24*, 197–201.
16. Ju, L.T.; Jhu, S.T. *The Antibacterial Influence of Seperates Out the Cupric Ion from the Stainless Steel*; Far East University: Vladivostok, Russia, 2004; pp. 707–717.
17. Chin-Min, C. *A Study on the Antibacterial Properties of Silver-Bearing 2205 Duplex Stainless Steels*; National Taiwan Ocean University: Keelung, Taiwan, 2010.
18. Lin, Z.D. *A Study on the Antibacterial Properties of Silver-Containing SUS 430 Stainless Steels*; National Taiwan Ocean University: Keelung, Taiwan, 2010.
19. Zeng, Y.S. *A Study on the Properties of Antibacterial Silver-Bearing 316L Stainless Steel*; National Taiwan Ocean University: Keelung, Taiwan, 2008.
20. Zhang, D.; Ren, L.; Zhang, Y.; Xue, N.; Yang, K.; Zhong, M. Antibacterial activity against *Porphyromonas gingivalis* and biological characteristics of antibacterial stainless steel. *Colloids Surf. B Biointerfaces* **2013**, *105*, 51–57. [CrossRef] [PubMed]
21. Chu, P.K. Enhancement of surface properties of biomaterials using plasma-based technologies. *Surf. Coat. Technol.* **2007**, *201*, 8076–8082. [CrossRef]
22. Díaz-Visurraga, J.; Guetierrez, C.; von Plessing, C.; García, A. Metal nanostructures as antibacterial agents. *Sci. Against Microb. Pathog. Commun. Curr. Res. Technol. Adv.* **2011**, 210–218.
23. Dunnill, C.W.H.; Aiken, Z.A.; Pratten, J.; Wilson, M.; Morgan, D.J.; Parkin, I.P. Enhanced photocatalytic activity under visible light in N-doped TiO_2 thin films produced by APCVD preparations using *t*-butylamine as a nitrogen source and their potential for antibacterial films. *J. Photochem. Photobiol. A Chem.* **2009**, *207*, 244–253. [CrossRef]
24. Zhang, W.; Liu, J.; Wang, H.; Xu, Y.; Wang, P.; Ji, J.; Chu, P.K. Enhanced cytocompatibility of silver-containing biointerface by constructing nitrogen functionalities. *Appl. Surf. Sci.* **2015**, *349*, 327–332. [CrossRef]
25. Hajipour, M.J.; Fromm, K.M.; Ashkarran, A.A.; de Aberasturi, D.J.; de Larramendi, I.R.; Rojo, T.; Serpooshan, V.; Parak, W.J.; Mahmoudi, M. Antibacterial properties of nanoparticles. *Trends Biotechnol.* **2012**, *30*, 499–511. [CrossRef] [PubMed]
26. Rana, S.; Kalaichelvan, P.T. Antibacterial activities of metal nanoparticles. *Adv. Biotech.* **2011**, *11*, 21–23.
27. Lu, M.Q.; Chen, S.H.; Dong, J.S.; Yang, K. Pilot study about the killing bacteria process and mechanism of ferrite antibacterial stainless steel. *Metallic Funct. Mater.* **2005**, *12*, 10–13.
28. Society, T.M.I. *ASM Handbook Volume 03—Alloy Phase Diagrams*; ASM International: Novelty, OH, USA, 1992.

29. Sung, J.H.; Kong, J.H.; Yoo, D.K.; On, H.Y.; Lee, D.J.; Lee, H.W. Phase changes of the AISI 430 ferritic stainless steels after high-temperature gas nitriding and tempering heat treatment. *Mater. Sci. Eng. A* **2008**, *489*, 38–43. [CrossRef]
30. Shen, Y.Z.; Kim, S.H.; Cho, H.D.; Han, C.H.; Ryu, W.S. Influence of tempering temperature upon precipitate phases in a 11% Cr ferritic/martensitic steel. *J. Nuclear Mater.* **2010**, *400*, 94–102. [CrossRef]
31. Mola, J.; de Cooman, B.C. Quenching and partitioning processing of transformable ferritic stainless steels. *Scr. Mater.* **2011**, *65*, 834–837. [CrossRef]
32. Erneman, J.; Schwind, M.; Liu, P.; Nilsson, J.O.; Andrén, H.O.; Ågren, J. Precipitation reactions caused by nitrogen uptake during service at high temperatures of a niobium stabilised austenitic stainless steel. *Acta Mater.* **2004**, *52*, 4337–4350. [CrossRef]
33. Zou, D.N.; Zhang, Z.; Zhang, S.L.; Bai, J.G.; Lin, Q.Z.; Han, Y. Effects of antibacterial treatment on microstructure and properties of copper-bearing ferrite stainless steel. *Foundry Technol.* **2005**, *26*, 1009–1011.
34. Yang, K.; Chen, S.H.; Dong, J.S.; Lu, M.Q. The antibacterial properties of ferrite antibacterial stainless steel. *Metallite Funct. Mater.* **2005**, *12*, 6–9.
35. Chieh, L.W. *A Study of the Antibacterial Property of the SUS430 Stainless Steel Containing Copper*; National Taiwan University: Taipei, Taiwan, 2000.
36. Shi, F.; Wang, L.; Cui, W.; Liu, C. Precipitation kinetics of Cr2N in high nitrogen austenitic stainless steel. *Iron Steel Res. Int.* **2008**, *15*, 72–77. [CrossRef]
37. Van Landeghem, H.P.; Gouné, M.; Redjaïmia, A. Nitride precipitation in compositionally heterogeneous alloys: Nucleation, growth and coarsening during nitriding. *J. Crystal. Growth* **2012**, *341*, 53–60. [CrossRef]